The performance analysis of direct methanol fuel cells with different hydrophobic anode channels

Hung-Chun Yeh[a], Ruey-Jen Yang[a], Win-Jet Luo[b,*], Jia-You Jiang[b], Yean-Der Kuan[b], Xin-Quan Lin[c]

[a] Department of Engineering Science, National Cheng Kung University, Tainan City 701, Taiwan
[b] Department of Refrigeration, Air Conditioning and Energy Engineering, National Chin-Yi University of Technology, No. 35, Lane 215, Sec. 1, Chung-Shan Rd., Taiping City, Taichung County 411, Taiwan
[c] Department of Chemical and Materials Engineering, National Chin-Yi University of Technology, Taiping City, Taichung County 411, Taiwan
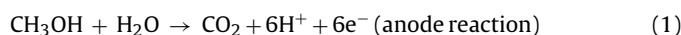
ARTICLE INFO

ABSTRACT

In order to enhance the performance of the direct methanol fuel cell (DMFC), the product of CO_2 bubble has to be efficiently removed from the anode channel during the electrochemical reaction. In this study, the materials of Polymethyl Methacrylate (PMMA) with hydrophilic property and polydimethylsiloxane (PDMS) with hydrophobic property are used to form the anode cannel. The channel is fabricated through a microelectromechanical system (MEMS) manufacture process of the DMFCs. In addition, some particles with high hydrophobic properties are added into the PDMS materials in order to further reduce the hydro-resistance in the anode channel. The performance of the DMFCs is investigated under the influence of operation conditions, including operation temperature, flow rate, and methanol concentration. It is found that the performance of the DMFC, which is made of PDMS with high hydrophobic particles, can be greatly enhanced and the hydrophobic property of the particles can be unaffected by different operation conditions.
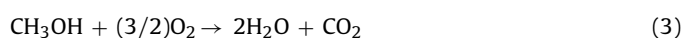
1. Introduction

Fuel cell is a type of energy conversion devices with high efficiency, which allows the electrochemical reaction between the fuel and oxidant to convert the chemical energy of the fuel directly into the electricity. The direct methanol fuel cell (DMFC), which utilizes the methanol solution as a fuel, has been considered as a promising power source for portable electronic devices. Methanol has high energy density and specific, superior chemical stability, which are important for transport and storage. Thus, compared with other fuel cell systems, the DMFC is a simple and compact system and also a potential power source for portable applications [1–3]. This reason has motivated researchers and industry engineers all over the world to study the DMFC. For example, the issue associated with the interactions between pairs of species in a multicomponent membrane was discussed in Refs. [4–8]. Refs. [9–12] investigated the design related to miniaturization. The open circuit voltage (OCV) and methanol cross-over problems were studied in Refs. [13,14]. Interaction between the catalytic materials of membranes and the fuel flow field was investigated in Refs. [15–17]. The physical parameters of the gas diffuse layer (GDL) such as the thickness, pore size and pore distribution, which affect the dynamics of two-phase transport had been studied extensively in Refs. [18–20]. The DMFC consists of a proton exchange membrane with an anode and a cathode catalyst layer on each side. Gas diffusion layers, usually made of carbon paper or carbon cloth, are used to cover the catalyst layers and form the membrane electrode assembly (MEA). The MEA is then sandwiched between two current collectors that have some flow channels machined on the surface for the supply of the fuel and oxidant. Typically, the DMFC is operated at a temperature lower than 100 °C. Methanol is electrochemically oxidized to CO_2 at the anode and oxygen is reduced to water at the cathode. The electrochemical reactions in the cell are described as follows:

$$CH_3OH + H_2O \rightarrow CO_2 + 6H^+ + 6e^- \text{ (anode reaction)} \tag{1}$$

$$(3/2)O_2 + 6H^+ + 6e^- \rightarrow 3H_2O \text{ (cathode reaction)} \tag{2}$$

The overall combined reaction is:

$$CH_3OH + (3/2)O_2 \rightarrow 2H_2O + CO_2 \tag{3}$$

Thus, the overall cell reaction is the electro-oxidation of methanol and water to CO_2. All of the reaction products, including gas CO_2 at the anode and liquid water at the cathode, should be removed from the electrode structure and cell as efficiently as possible to maintain an effective continuous reaction. Similar to the water management at the cathode, the efficient removal of CO_2 at the anode is one of the most important research issues in the development of DMFCs.

* Corresponding author. Tel.: +886 6 23924505x8255; fax: +886 6 23932758.
E-mail address: wjluo@ncut.edu.tw (W.-J. Luo).

In the DMFC, methanol solution is fed into the anode flow field and diffuses into the catalyst sites through the gas diffusion layer, while the reaction-produced gas CO_2 at the catalyst layer is transported backward into the anode channels through the gas diffusion layer. Consequently, a counter liquid–gas two-phase flow takes place in the diffusion layer. When the quantity of CO_2 increases at high current density range, the volume fraction of CO_2 in the anode flow field becomes rather large. In such a situation, CO_2 removal from the catalyst sites is critical to ensure the availability of an adequate surface area for methanol oxidation. To this end, CO_2 has to be removed effectively from both the diffusion layer and the anode flow field. Otherwise, stagnant CO_2 gas slugs that adhere to the surface of the diffusion layer may block the pores, which in turn hinder the diffusion of methanol solution to the catalyst layer. The diffusion may also cause a higher pressure in the anode flow field, leading to an increase in methanol cross-over. Consequently, this result can lead to the starvation of the reaction sites and severe cell performance loss. Hence, the investigation on the removal of CO_2 gas bubbles at the anode channels will serve as a guide for improvement on the performance of DMFC.

Some studies have reported CO_2 bubble behavior in the anode flow field of DMFCs. Mench et al. [21] examined gas bubble growth and ejection from the backing layer and flow channel interface region with video microscopy and observed discrete bubbles on the order of 0.1–0.5 mm evolving from various locations within the backing layer. Argyropoulos et al. [22] investigated visually the CO_2 gas evolution process inside an operating DMFC. The effects of operating parameters including different gas diffusion layer supporting materials, flow bed designs, cell sizes, exhaust manifold configurations, and the current density on the system gas management are investigated. Scott et al. [23] visually investigated the CO_2 gas evolution and flow behavior with flow beds based on a stainless steel mesh. In their study, a number of the flow designs, based on stainless steel mesh, showed promising behavior in terms of gas removal characteristics and electrical performance. Yang et al. [24] reported a visual study of CO_2 bubble behavior in a single serpentine channel of a transparent DMFC anode. The study revealed the influence of current densities, cell orientation, methanol solution flow rates, and CO_2 bubble distribution for different serpentine channels and parallel channels at different current densities [24,25]. Bewer et al. [26] reported a novel method of simulating two-phase flow in a DMFC using an aqueous H_2O_2 solution. The influence of the flow field on the bubble formation and flow homogeneity, as well as the influence of the manifold on the flow homogeneity, was investigated. Lu and Wang [27] developed a $5\,cm^2$ transparent DMFC to visualize CO_2 bubble flow in the anode and investigated the effects of pore structure and wettability on two-phase flow dynamics.

In this paper, a visual investigation of CO_2 gas bubble behavior in a transparent DMFC with the anode flow field consisting of three parallel serpentine channels is presented. The dynamic behavior of CO_2 gas bubbles in the anode channels of the operating cell was recorded in situ, and polarization curves were obtained to provide a fundamental understanding of the relationship between the hydrophobic character of the anode channel and the cell performance. A series of parametric studies, including the aqueous methanol solution flow rate, temperature, and concentration were performed to evaluate the effects of CO_2 gas bubble behavior in different hydrophobic anode channels as well as on the cell performance.

2. Experimental

2.1. Transparent cell

Fig. 1 shows the exploded view of the transparent DMFC test fixture designed and fabricated for the visualization study in this paper. The MEA, which is detailed in the subsequent paragraph, was sandwiched between two bipolar plates with a gasket onto either side of the MEA. This assembly, including the bipolar plates and MEA, was clamped between two enclosure plates by using eight M8 screw joints (each having a torque of about 12 KGF-CM). The active area of the MEA adopted in this paper is 3.5 cm × 3.5 cm, which consisted of two single-side ELAT electrodes from E-TEK and a Nafion® membrane 117. Both anode and cathode electrodes used carbon cloth (E-TEK, Type A) as the backing support layer with 30% PTFE wet-proofing treatment. The catalyst loading on the anode side was $4.0\,mg\,cm^{-2}$ with unsupported [Pt:Ru] Ox (1:1 a/o), while the catalyst loading on the cathode side was $2.0\,mg\,cm^{-2}$ with 40% Pt on Vulcan XC-72. Furthermore, $0.8\,mg\,cm^{-2}$ Nafion® was applied to the surface of each electrode. The bipolar plates (shown in Fig. 1) were made of 316 stainless steel [28–31] plates with a thickness of 2.0 mm in order to avoid corrosion. As shown in Fig. 1, the rectangular bipolar plate consisted of two portions: the channel area and the extension area. The channel area acted as the distributor for supplying fuel and oxidant to the MEA. The three parallel serpentine channels, having an area of 2.0 mm × 2.0 mm, were machined using the wire-cut technology. The width of the ribs was 2 mm.
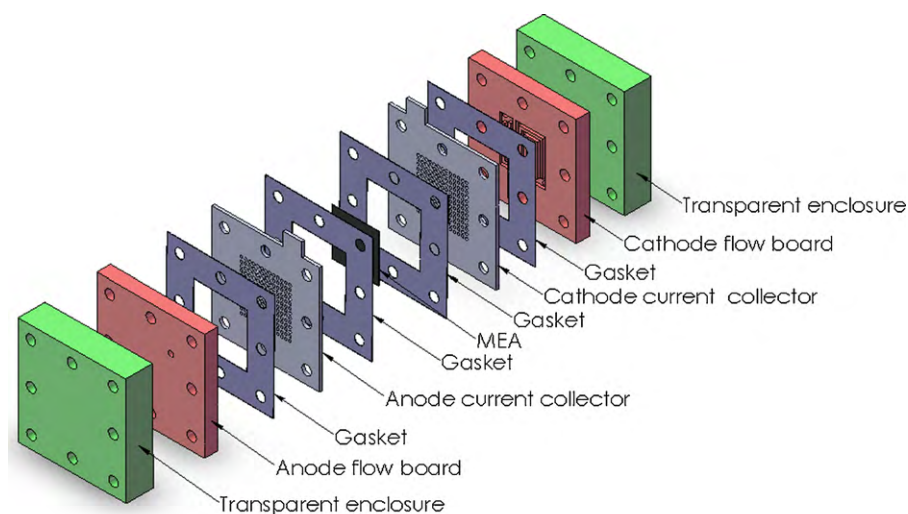

Fig. 1. Exploded view of the transparent DMFC test fixture.

The serpentine channel comprised a total length of 676 mm. The extension area of the bipolar plates served as a current collector. In addition, a tape heater was attached to the extension area to adjust the cell operation temperature to a desired value during the experiments. For the purpose of visualization, the two enclosure plates (2.0 cm thick) were made of transparent Lucite material. The two-phase flow characteristics of gas CO_2 and methanol solution in the anode flow field could be distinctly visualized and recorded by the image recording system through the transparent enclosure plate. Notice that the transparent Lucite material, having a well-insulated property, can effectively keep the heat in the MEA and the bipolar plates from dissipating to the surroundings under higher operation temperatures.

2.2. The fabrication of the PDMS channels

Soft lithography is a diverse set of techniques that encompasses replica molding using an elastomeric material, specifically polydimethylsiloxane (PDMS), for the fabrication of microfluidic devices as well as for the patterning of surfaces using PDMS stamps (microcontact printing). The common procedure used for making PDMS channels involves the fabrication of a silicon master with patterned features composed of a photoresist (SU-8). In this process, silicon wafers were coated with photoresist and then exposed to ultraviolet (UV) light through a mask with the desired pattern. High-resolution transparencies were used as the photomask to rapid prototype SU-8 patterned masters, from which PDMS molds can be replicated. In the fabrication process, silicone elastomer and elastomer curing agent (Sil-More Industrial Ltd., USA Sylgard 184A and Sylgard 184B) were mixed in a ratio of 10:1 and then poured onto an SU-8 mold. The interrelated fabrication process can refer to Luo [32,34]. The PDMS was cured at a temperature of 70 °C for 1 h and then treated using oxygen plasma to change its inherent hydrophobic surface property to a hydrophilic property. The PDMS inverse structure was then peeled off the template. Full details of the fabrication process are presented in Refs. [32–35].

2.3. Test loop

The schematic of the experimental setup is shown in Fig. 2. Methanol solution was driven by a squirm pump, which can precisely control the liquid flow rate from 3 to 15 ml/min with an error of 2%. Before entering the cell, methanol solution was pre-heated to a desired temperature by placing the methanol solution tank in a temperature controllable water bath. The mixture of gas CO_2 and unreacted methanol solution was drained from the cell and cooled down when passing through a cooling system. The gas (CO_2) produced at anode was separated from the methanol solution tank and released to the atmosphere, while the unreacted methanol solution was re-collected into a chemical liquid tank. Simultaneously, the ambient air with almost 80% oxygen as oxidant was provided to the cathode side of the cell without humidification. The flow rate of oxygen was controlled by an air mass flow regulator, which has an error of 5% of the full scale.

3. Results and discussion

The performance of the DMFC is seriously affected by the CO_2 bubbles (the electrochemical reaction product) in the anode channel. The CO_2 bubbles must be efficiently removed from the anode channel to maintain continuous power generation efficiency. In this study, the materials of PMMA and PDMS, with different hydrophobic properties, were used as the substrates of the anode channels of the DMFCs, which were fabricated via MEMS fabrication. The effect of hydro-resistance for the supply fuel in the anode channels was modulated by using different hydrophobic materials as anode channel substrates.

By using a highly hydrophobic material, PDMS, the hydro-resistance in the anode channel was smaller, and the product of the CO_2 bubble could be easily removed from the anode channel. In order to further reduce the hydro-resistance in the anode channel, small particles of Mobil Composition of Matters-41 (MCM-41) having a higher hydrophobic property were uniformly added into the PDMS substrate. A CCD camera was used to capture the CO_2 bubble removal procedures. Due to the reflection of the liquid–gas interface, the CO_2 bubble formation, growth, and motions in the flow channel were distinctly captured by the image recording system, as shown in Figs. 3 and 4. With the help of a lighter liquid–gas interface, gas bubbles could be easily distinguished from liquid methanol solution. The region enveloped by a lighter-grey liquid–gas interface represents a gaseous area, whereas the remaining region in the flow field is the liquid area. At each active nucleation site, gas bubbles formed, grew, and departed from the surface of the diffusion layer with the help of the cross current flow of the methanol solution. For a given operation condition, the process of bubble formation and departure was repeated period-
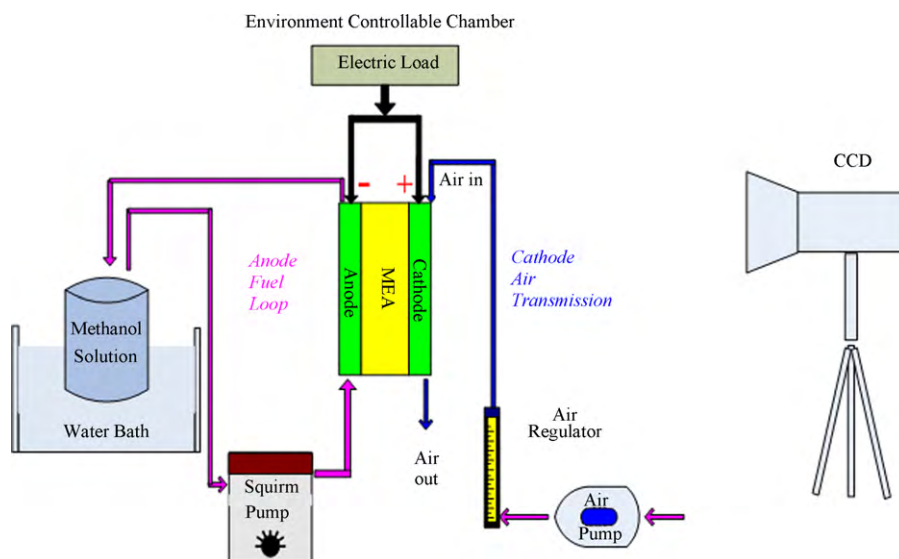

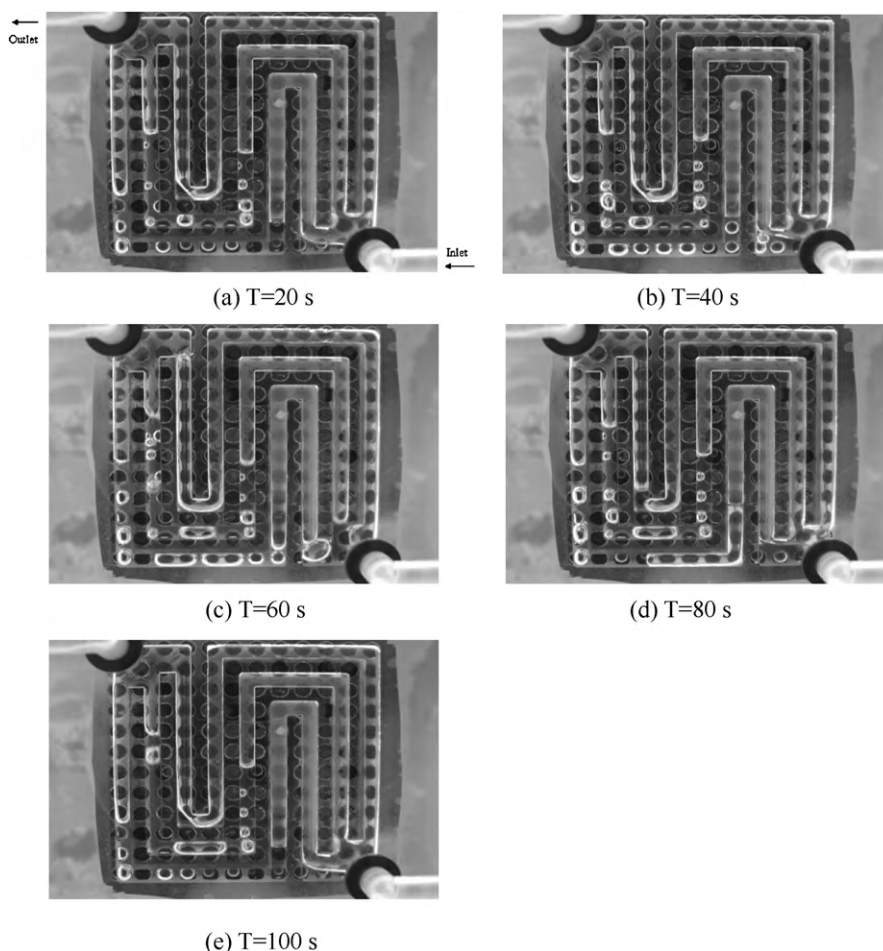**Fig. 2.** Schematic of the experimental setup.

(a) T=20 s

(b) T=40 s

(c) T=60 s

(d) T=80 s

(e) T=100 s

Fig. 3. CO_2 bubble behavior using PMMA as the substrate.

ically. After departing from the surface of the gas diffusion layer, the small and spherical gas bubbles traveled upwards to the upper surface of the channel due to buoyancy. The gas bubbles then moved towards the outlet of the flow field with the liquid methanol solution. Traveling along the flow channel towards the outlet, the bubbles gradually grew via coalescing with the newly produced small bubbles from the surface of the gas diffusion layer. Fig. 3 demonstrates the CO_2 bubble behavior with an increase in reaction time for the case of PMMA as the substrate under a selected current density ($90\,mA\,cm^{-2}$). The cell was oriented vertically and with 10% methanol solution supplied at a flow rate of $10\,cm^3\,min^{-1}$ at $55\,°C$. As shown in Fig. 3, the upper serpentine channel in the anode channel was almost filled with slug bubble due to the buoyancy of the gas bubble. At 80 s, the long slung bubble was divided into two segments in the lower left corner of the upper serpentine channel. As time elapsed, the shorter slug near the outlet was pushed out of the anode channel. The right, longer slug was pushed forward and occupied the entire upper serpentine channel again as shown in Fig. 3(e). However, in the middle and lower serpentine channels, the slug bubbles occupied only the right side of the two channels and a rather small number of discrete gas bubbles were generated and were present in the downstream region of the channels. As time elapsed, some of small spherical bubbles gradually enlarged and eventually became slug bubbles. Unlike the small spherical bubbles, slug bubbles are usually long and span the entire channel cross-section. As time further elapsed, the new product slug in the lower left region of the lower serpentine channel gradually moved towards the original long slug near the inlet of the channel, and the two slugs merged eventu-

ally, at 80 s. Then, the merged long slug became divided into two segments in the lower right corner of the lower serpentine channel. At 100 s, the shorter slug in the lower region of the cell was pushed out of the anode channel. In Fig. 3(a)–(e), it can be seen that rather long gas slugs formed and occupied almost half of the area of the serpentine channels and the entire channel cross-section. This formation caused the effective contact area between the liquid fuel and the gas diffusion layer to be extremely small. Under such a condition, the long gas slugs may restrict the continuous supply of methanol through the gas diffusion layer to the catalyst surface, eventually leading to the deterioration of the mass transfer of methanol. Fig. 4 presents the images of the CO_2 bubble behavior with the increase in reaction time. PDMS was used as the substrate under a selected current density ($108\,mA\,cm^{-2}$) when the cell was oriented vertically and with 10% methanol solution supplied at a flow rate of $10\,cm^3\,min^{-1}$ at $55\,°C$. As shown in the figure, a rather small number of discrete gas bubbles were generated and distributed uniformly over the whole anode channel at 35 s. At 60 s, some of the small spherical bubbles gradually enlarged, merged together, and eventually became segmental slug bubbles occupying the upper and middle serpentine channels. At 75 s, due to lower hydro-resistance in the anode flow, these segmental slugs were pushed forward by the pressure from the supplied methanol and were progressively removed from the anode channel.

The bubble removal rates from the anode channels with the increase in electrochemical reaction time were illustrated by calculating the bubble covering area in the anode channel (shown in Fig. 5). The bubble covering area is relative to the growing size
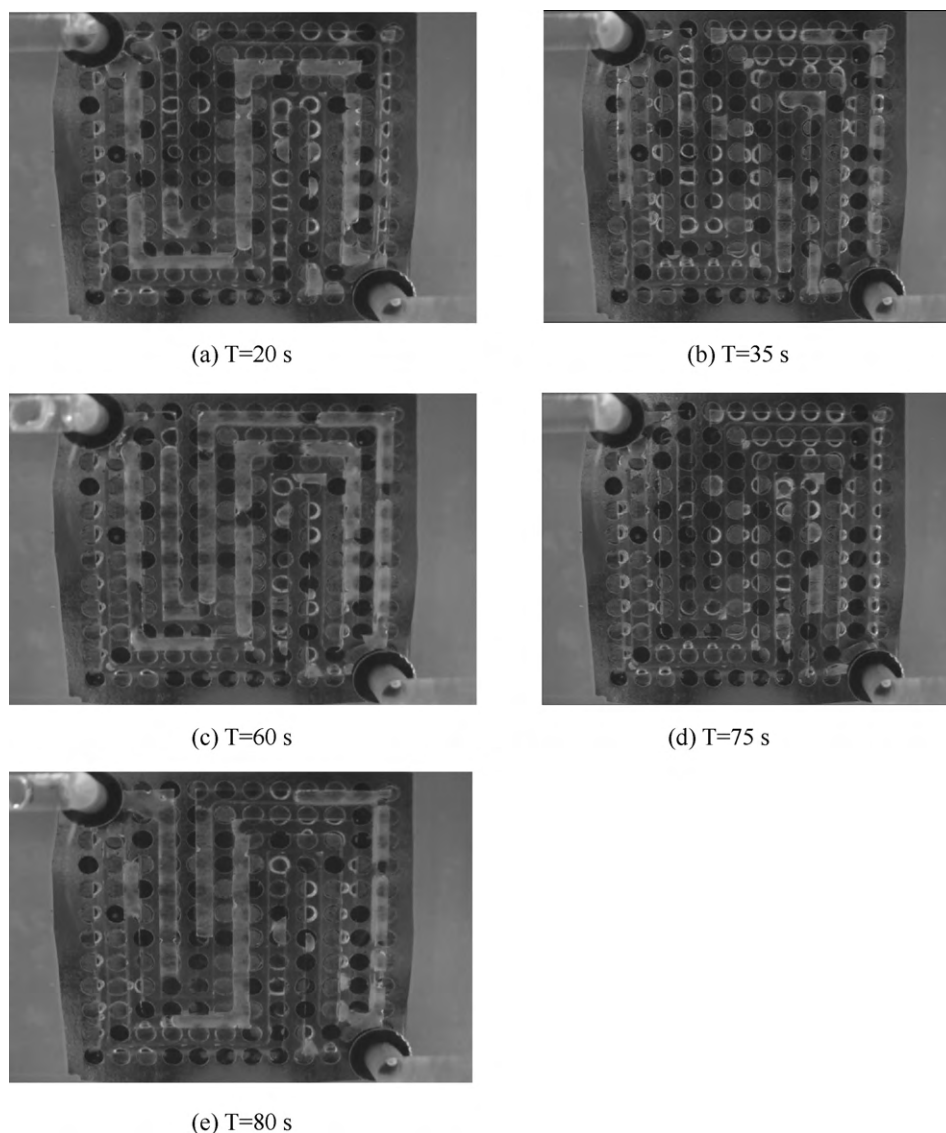
(a) T=20 s   (b) T=35 s

(c) T=60 s   (d) T=75 s

(e) T=80 s

Fig. 4. CO_2 bubble behavior using PDMS as the substrate.

of the bubbles and their halting periods in the anode channels. When the bubbles gradually grew in size, the area covering the bubbles also gradually increased. These gradually growing bubbles obstructed the anode channels and restricted the continuous supply of methanol to the catalyst. The area covering the bubbles then further increased. When the driving force from the supplied methanol surpassed the hydro-resistant force in the anode channel, the bubbles were pushed downwards and flowed out of the anode channels. As a result, the bubble covering area gradually decreased. For PDMS, the distribution of the bubble covering area elevated and fell noticeably, as shown in Fig. 5. Thus, due to lower hydro-resistance in the anode channel, the driving force from the supplied methanol surpassed the hydro-resistance force easily, and the bubbles were easily pushed forward with increasing covering area. When the bubbles flowed out the anode channel, the covering area decreased suddenly. However, when PMMA was used, the distribution of the bubble covering area appeared more smoothly and gradually increased with the electrochemical reaction time in comparison with the former case (shown in Fig. 5). This phenomenon indicates that the hydro-resistance in the anode channel was greater and the halting time of the bubble was longer in comparison with the former case. The max-

imum covering area in the anode channel could reach a value of 84% at 70 s from the beginning of the electrochemical reaction.

The efficiencies of the DMFCs with different hydrophobic anode channels were also investigated under the influence of the environmental temperatures (30–70 °C), the fuel supply flow rates in the anode channels (3–15 cm^3 min^{-1}), and the solution concentration of the methanol in pure water (5–20%).

3.1. The effect of the operation temperature on the efficiency of the DMFCs

Fig. 6 illustrates the distributions of the power density for the three different hydrophobic materials as substrates under the operation conditions of 30 °C, 10 cm^3 min^{-1}, and a 10% methanol concentration. Due to lower hydro-resistance in the anode channel for MCM-41 particles uniformly added into the PDMS substrate (PDMS1), the new small CO_2 bubbles produced in the anode channel were easily pushed forward and removed from the anode channel. As the result, the power density for the case was the greatest among the three cases under any specific load and reached a maximum value of 21.6 mW cm^{-2}, as shown in the figure. How-
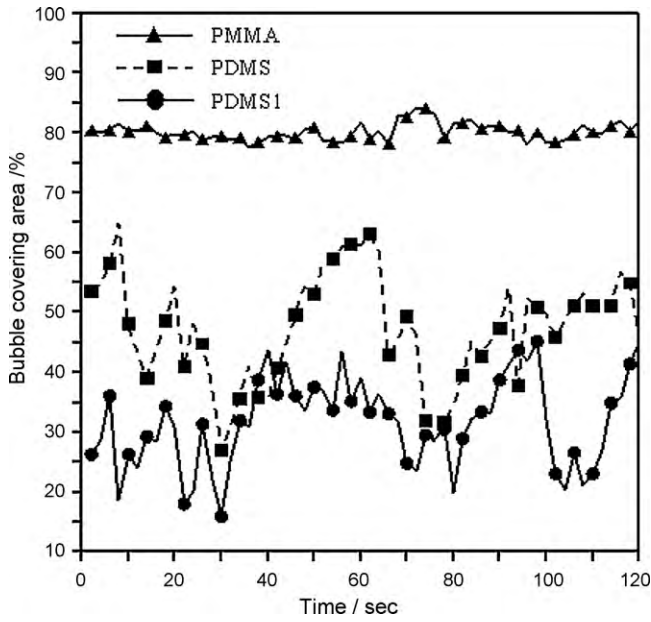
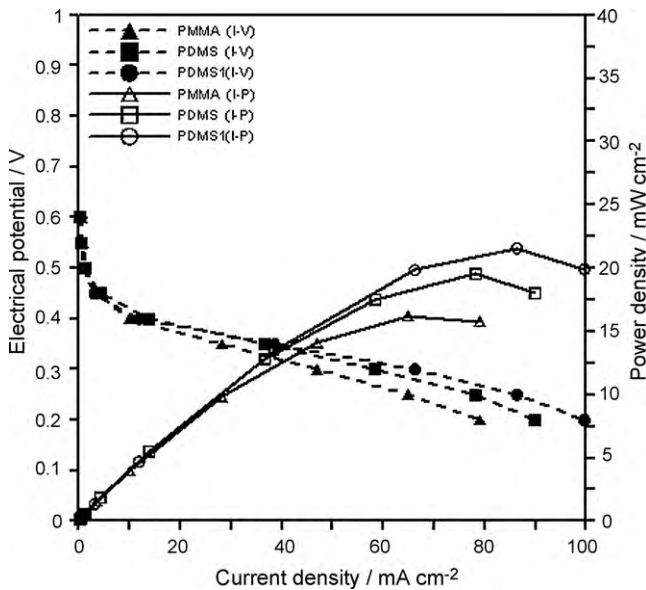**Fig. 5.** Distribution of the bubble converting area in the anode channels.

Fig. 6. Power densities for the DMFCs under the operation condition of 10% methanol solution supplied at flow rate of $10\,cm^3\,min^{-1}$ at 30 °C.
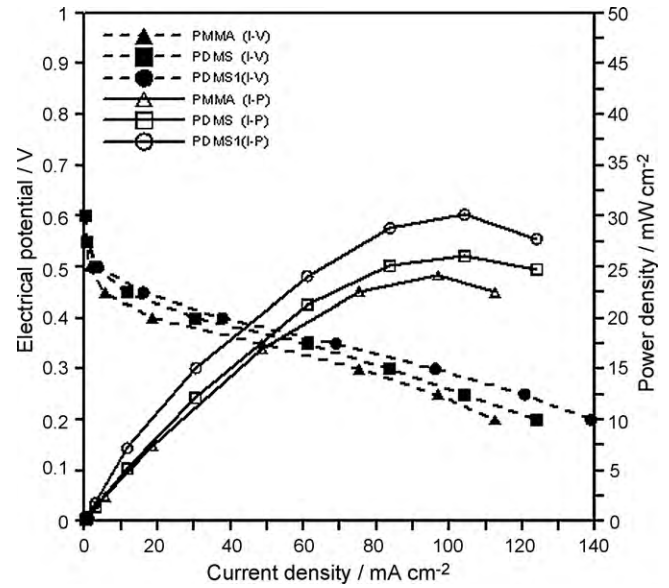

Fig. 7. Power densities for the DMFCs under the operation condition of 10% methanol solution supplied at flow rate of $10\,cm^3\,min^{-1}$ at 70 °C.

Table 1

Maximum power density of the DMFCs with an increasing operation temperature under the conditions of a $10\,cm^3\,min^{-1}$ flow rate and a 10% methanol concentration.

Temperature (°C)	Material		
	PMMA ($mW\,cm^{-2}$)	PDMS ($mW\,cm^{-2}$)	PDMS1 ($mW\,cm^{-2}$)
30	16.220	19.552	21.573
55	19.771	23.070	25.698
70	24.184	26.038	30.156

conditions of 70 °C, $10\,cm^3\,min^{-1}$, and a 10% methanol concentration. By comparing the results in Figs. 6 and 7, the maximum power densities for the three cases all increased with an increasing temperature from 30 to 70 °C. Tables 1 and 2 show the maximum power densities and corresponding differences in the three cases at a flow rate of $10\,cm^3\,min^{-1}$ and a methanol concentration of 10% at different operation temperatures. The power density differences, comparing PDMS and PMMA with PDMS1 and PMMA, both gradually decreased with the increase in the operation temperature. This phenomenon indicates that the increasing operation temperature weakened the effect of hydro-resistance reduction in the hydrophobic anode channel. However, the power density difference between PDMS and PDMS1 gradually increased with the increase in the operation temperature. For the hydrophobic particles, the effect of hydro-resistance reduction was essential for increasing the operation temperatures.

3.2. The effect of the fuel flow rate on the efficiency of the DMFCs

Figs. 8 and 9 illustrate the distributions of the power density for the three cases with fuel flow rates of 3 and $15\,cm^3\,min^{-1}$, respectively, under the operation condition of 55 °C and a 10% methanol concentration. When the flow rate increased, the power densities
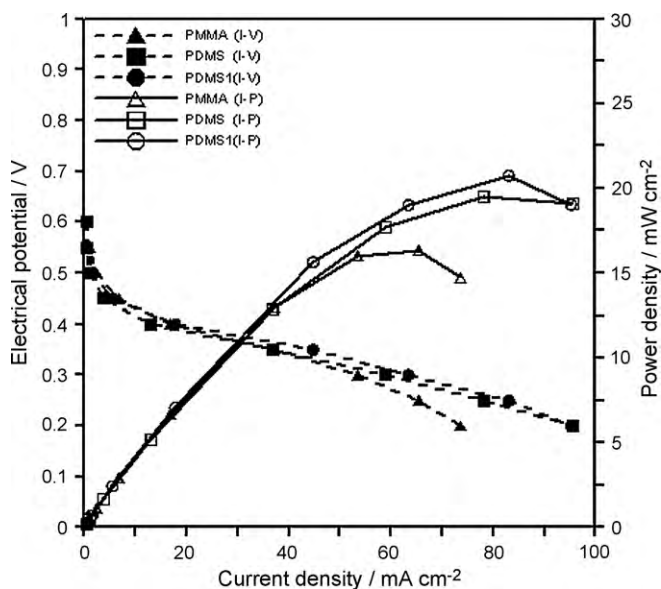
ever, for PMMA, the hydro-resistance in the anode channel was the greatest among the three cases. The small CO_2 bubbles left the catalyst layer and gradually grew. The neighboring bubbles merged into a slug form and halted in the anode channel over longer periods. Thus, the power density for this case attained a maximum value of only $16.2\,mW\,cm^{-2}$. From the figure, the deviations of the power densities between PDMS and PDMS1 are not apparent under the operation conditions. Fig. 7 shows the distributions of the power density for the three cases under the operation

Table 2

Differences of the maximum power densities for the DMFCs under a $10\,cm^3\,min^{-1}$ flow rate and conditions of 30 °C, 55 °C, 70 °C and a 10% methanol concentration.

Temperature (°C)	((PDMS − PMMA)/PMMA) × 100 (%)	((PDMS1 − PMMA)/PMMA) × 100 (%)	((PDMS1 − PDMS)/PDMS) × 100 (%)
30	20.5	33	10.3
55	16.7	30	11.4
70	7.6	24.7	15.8

Fig. 8. Power densities for the DMFCs under the operation condition of a 10% methanol solution supplied at flow rate of 3 cm^3 min^{-1} at 55 °C.
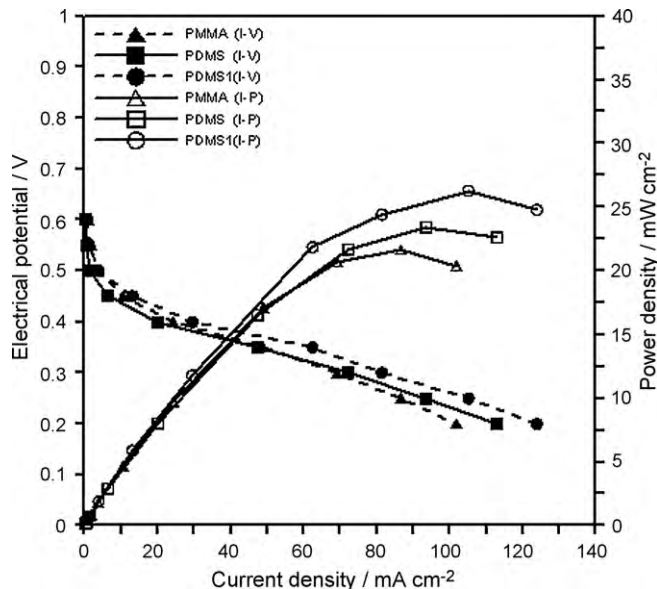

Fig. 9. Power densities for the DMFCs under the operation condition of a 10% methanol solution supplied at flow rate of 15 cm^3 min^{-1} at 55 °C.

Table 3
Maximum power density of the DMFCs with an increasing flow rate under conditions of 55 °C and a 10% methanol concentration.

Flow rate (cm^3 min^{-1})	Material		
	PMMA (mW cm^{-2})	PDMS (mW cm^{-2})	PDMS1 (mW cm^{-2})
3	16.320	19.511	20.749
10	19.771	23.070	25.698
15	21.633	23.401	26.271
20	–	–	–

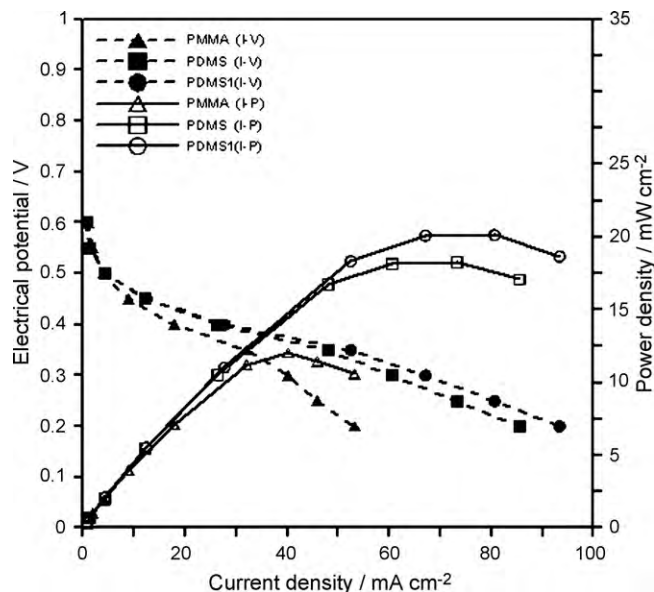**Fig. 10.** Power densities for the DMFCs under the operation condition with a 5% methanol solution supplied at a flow rate of 10 cm^3 min^{-1} at 55 °C.

flow rate resulted in an increase in the power density difference. Thus, the hydro-resistance effect of hydrophobic particles was not significantly affected by the increase of the flow rate. When the flow rate was greater than 20 cm^3 min^{-1}, the effect of methanol flow cross-over between anode and cathode sides became significant. The power density of the DMFC under this condition was not measured in this study.

3.3. The effect of the methanol concentration on the efficiency of the DMFCs

Figs. 10 and 11 illustrate the distributions of the power densities for the three cases with methanol concentrations of 5% and 10%, respectively, under the operation condition of 55 °C and a 10 cm^3 min^{-1} flow rate. From the two figures, the increase in the methanol concentration from 5% to 10% resulted in power density increases in the three cases due to the greater amount of methanol fuel supplied for the electrochemical reaction. The electric power-generating performance of PDMS1 was also the best among the three cases. The power density reached a maximum value of 25.7 mW cm^{-2} at a 10% methanol concentration.

all increased in the three cases due to the supply of more methanol fuel. The electric power-generating performance of PDMS1 was the best among the three cases under different flow rates. As shown in Tables 3 and 4, the power density differences between PDMS and PMMA and between PDMS1 and PMMA had maximum values at the flow rate of 10 cm^3 min^{-1}. Thus, the hydro-resistance reduction effect was not significant at a high flow rate of the supply methanol. However, for PDMS and PDMS1, the increase in the

Table 4
Differences in the maximum power densities for the DMFCs with flow rates of 3 cm^3 min^{-1}, 10 cm^3 min^{-1}, 15 cm^3 min^{-1}, and 20 cm^3 min^{-1}, using 55 °C and a 10% methanol.

Flow rate (cm^3 min^{-1})	((PDMS − PMMA)/PMMA) × 100 (%)	((PDMS1 − PMMA)/PMMA) × 100 (%)	((PDMS1 − PDMS)/PDMS) × 100 (%)
3	16.3	27.1	10.4
10	16.7	30	11.3
15	8.1	21.4	12.3
20	–	–	–

Table 5
Maximum power density of the DMFCs with an increasing the methanol concentration under conditions of 55 °C and a 10 cm^3 min^{-1} flow rate.

Concentration (%)	Material		
	PMMA (mW cm^{-2})	PDMS (mW cm^{-2})	PDMS1 (mW cm^{-2})
5	11.478	18.284	20.136
10	19.771	23.070	25.698
15	19.181	21.711	22.148
20	17.244	19.090	20.256

Table 6
Differences of the maximum power densities for the DMFCs at 55 °C and a 10 cm^3 min^{-1} flow rate, with 3%, 10%, 15%, or 20% methanol concentrations.

Concentration (%)	((PDMS − PMMA)/PMMA) × 100 (%)	((PDMS1 − PMMA)/PMMA) × 100 (%)	((PDMS1 − PDMS)/PDMS) × 100 (%)
5	59.3	75.4	10.1
10	16.7	30	11.4
15	13.2	15.5	2
20	10.7	17.5	6.1
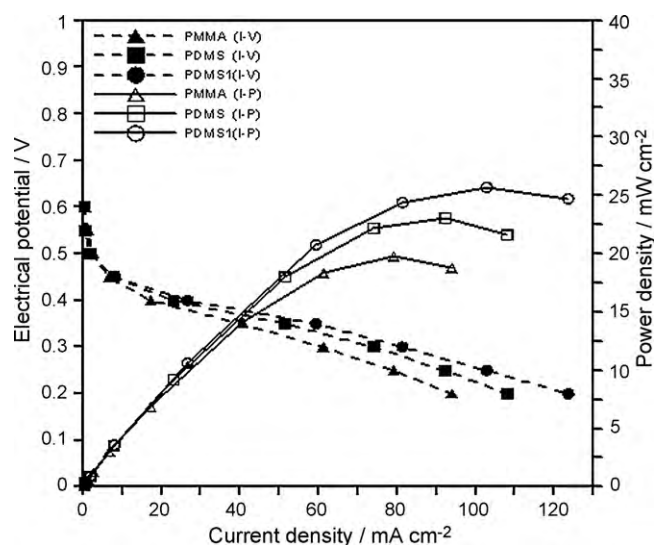
Fig. 11. Power densities for the DMFCs under the operation condition of a 10% methanol solution supplied at a flow rate of 10 cm^3 min^{-1} at 55 °C.

Tables 5 and 6 show the maximum power densities and differences in the three cases at different supply methanol concentrations under the operation condition of 55 °C and a 10% methanol concentration. In Table 5, when the methanol concentration increased from 10% to 20%, the power densities in the three cases gradually decreased with the increase in the methanol concentration due to methanol flow cross-over from anode to cathode side. Under the condition of a 10% methanol concentration, the maximum power densities in the three cases all reached maximum values. However, the power density differences between PDMS and PMMA and between PDMS1 and PMMA gradually decreased with the increase in the methanol concentration from 5% to 20%. This phenomenon indicates that increasing the concentration of the supply methanol solution can weaken the effect of the hydro-resistance reduction in the hydrophobic anode channel. However, in comparison with PDMS and PDMS1, with a methanol concentration below 10%, the effect of the hydro-resistance reduction for hydrophobic particles was significant (as shown in Table 6).

4. Conclusions

This study investigated the CO_2 bubble removal effect and the corresponding electric output of the DMFCs with different hydrophobic anode channels made of PMMA and PDMS. PMMA material is transparent and hydrophilic, and PDMS mate-

rial is transparent and hydrophobic. The hydro-resistance in the hydrophobic anode channel is much smaller than that in the hydrophilic anode channel. In order to further reduce the hydro-resistance in the anode channel, hydrophobic micro-particles (MCM-41) were uniformly added into PDMS. DMFCs with an anode channel made of different materials mentioned above were tested under different operating conditions, including temperature, fuel flow rate, and solution concentration of the supplied fuel. The CO_2 bubble removal effect and the electric output of the DMFC made of PDMS anode channels possessing the hydrophobic particles were always best among the DMFCs under any of the specific operating conditions tested. However, the increase in the operation temperature, fuel flow rate, and solution concentration resulted in decreased hydro-resistance reduction effect of PDMS. In comparison with PDMS, the properties of the hydrophobic particles were more stable under these operation conditions. When hydrophobic particles were used in the PDMS anode channel, the CO_2 removal effect and the electric output of the DMFC were not significantly affected by the increase in these operation conditions. The performance of the DMFC still possessed a high efficiency when the operation conditions were varied. At the operation condition of 55 °C, 10 cm^3 min^{-1}, and a 5% methanol solution, a maximum difference in the electric outputs of the DMFCs was achieved. The electric output of the PDMS1 DMFC was 1.75 times greater than the PMMA DMFC. The PDMS anode channels can closely adhere to the anode current collector and prevent the fuel leakage from the anode channels. Otherwise, the PDMS anode channels are easily fabricated by using polymerization in a mold such is fully potential in mass production.

Acknowledgment

References

[1] C.K. Dyer, J. Power Sources 106 (2002) 31–34.
[2] T. Schultz, S. Zhou, K. Sundmacher, Chem. Eng. 24 (2001) 12.
[3] R. Dillon, S. Srinivasan, A.S. Aricò, V. Antonucci, J. Power Sources 127 (2004) 112–126.
[4] J.P. Meyers, J. Newman, J. Electrochem. Soc. 149 (6) (2002) A710–A717.
[5] J.P. Meyers, J. Newman, J. Electrochem. Soc. 149 (6) (2002) A718–A728.
[6] J.P. Meyers, J. Newman, J. Electrochem. Soc. 149 (6) (2002) A729–A735.
[7] A.H. Wang, C.Y. Wang, J. Electrochem. Soc. 150 (4) (2003) A508–A519.
[8] H. Dohle, J. Divisek, R. Jung, J. Power Sources 86 (2000) 469–477.
[9] G.Q. Lu, C.Y. Wang, T.J. Yern, X. Zhang, Electrochim. Acta 49 (2004) 821–828.
[10] J. Yu, P. Cheng, Z. Ma, B. Yi, J. Power Sources 124 (2003) 40–46.

[11] J.C. Amphlett, B.A. Peppley, E. Halliop, A. Sadiq, J. Power Sources 96 (2001) 204–213.
[12] A. Blum, T. Duvdevani, M. Philosoph, N. Rudoy, E. Prlrd, J. Power Sources 117 (2003) 22–25.
[13] Z. Qi, A. Kaufman, J. Power Sources 110 (2002) 177–185.
[14] R. Jiang, D. Chu, J. Electrochem. Soc. 151 (1) (2004) A69–A76.
[15] K. Scott, W.M. Taama, P. Argyropoulos, J. Power Sources 79 (1999) 43–59.
[16] N. Nakagawa, Y. Xiu, J. Power Sources 118 (2003) 248–255.
[17] X. Ren, T.E. Springer, T.A. Zawodzinski, S. Gottesfeld, J. Electrochem. Soc. 147 (2) (2000) 466–474.
[18] J. Nordlund, A. Roessler, G. Lindbergh, J. Appl. Electrochem. 32 (2002) 259–265.
[19] Z. Qi, M. Hollett, C. He, A. Attia, A. Kaufman, Electrochem. Solid-State Lett. 6 (2) (2003) A27–A29.
[20] H. Dohle, R. Jung, N. Kimiaie, J. Mergel, M. Müller, J. Power Sources 124 (2003) 371–384.
[21] M.M. Mench, S. Boslet, S. Thynell, J. Scott, C.Y. Wang, Proceedings of the Symposium on Direct Methanol Fuel Cells, The 199th Electrochem. Soc. Proc. Series, Princeton, NJ, 2001.
[22] P. Argyropoulos, K. Scott, W.M. Taama, Electrochim. Acta 44 (1999) 3575–3584.
[23] K. Scott, P. Argyropoulos, P. Yiannopoulos, W.M. Taama, J. Appl. Electrochem. 31 (2001) 823–832.
[24] H. Yang, T.S. Zhao, Q. Ye, J. Power Sources 139 (2005) 79–90.
[25] H. Yang, T.S. Zhao, Electorchim. Acta 50 (2005) 3243–3252.
[26] T. Bewer, T. Beckmann, H. Dohle, J. Mergel, D. Stolten, J. Power Sources 125 (2004) 1–9.
[27] G.Q. Lu, C.Y. Wang, J. Power Sources 134 (2004) 33–40.
[28] J. Ihonen, F. Jaouen, G. Lindbergh, G. Sundholm, Electrochim. Acta 46 (2001) 2899–2911.
[29] D.P. Davies, P.L. Adcock, M. Turpin, S.J. Rowen, J. Power Sources 86 (2000) 237–242.
[30] D.P. Davies, P.L. Adcock, M. Turpin, S.J. Rowen, J. Appl. Electrochem. 30 (2000) 101–105.
[31] E. Middelman, W. Kout, B. Vogelaar, J. Power sources 118 (2003) 44–46.
[32] W.J. Luo, Microfluidics Nanofluidics 6 (2009) 189–602.
[33] W.J. Luo, K.F. Yarn, M.H. Shin, K.C. Yu, Optoelectron. Adv. Mater. Rapid Commun. 2 (2) (2008) 117–125.
[34] Y.J. Pan, J.J. Lin, W.J. Luo, R.J. Yang, Biosens. Bioelectron. 21 (8) (2006) 1644–1648.
[35] G.S. Fiorini, D.T. Chiu, BioTechniques 38 (2005) 429–446.